Polymer 348 (2026) 129732

Contents lists available at ScienceDirect

Polymer

journal homepage: www.elsevier.com/locate/polymer

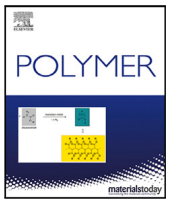

Assessment of reactive force fields for the failure of hydrocarbon chains: Insights from molecular dynamics and density functional theory☆

Luca Liu[1], Guido Raos*

Department of Chemistry, Materials and Chemical Engineering "G. Natta", Politecnico di Milano, via E. Bassini 6, 20133, Milano, Italy

ARTICLE INFO

Keywords:
Polymer mechanics
Molecular dynamics
reactive force fields

ABSTRACT

Understanding the mechanical behavior of polymer chains at the molecular level is essential for predicting also their bulk properties, including fracture. Here we investigate the tensile elasticity and failure of single polyethylene (PE) chains using both molecular dynamics (MD) simulations and quantum chemical calculations. Simulations were performed on a long PE chain ($C_{202}H_{406}$) to assess the differences between four reactive force fields (AIREBO, MEAM, ci-ReaxFF and ReaxFF), while a shorter chain ($C_{16}H_{34}$) was used for direct comparison of the force fields with density functional theory (DFT). Our results indicate that ReaxFF and ci-ReaxFF closely replicate the DFT predictions and approach the available experimental data for the work of fracture of long hydrocarbon chain. AIREBO consistently overestimates failure forces in both molecular dynamics and energy minimization, while the MEAM predictions depend on the computational method: it underestimates failure forces in molecular dynamics simulations but significantly overestimates them in minimization calculations. These findings suggest that ReaxFF and ci-ReaxFF are reliable choices for simulating the scission of polymer chains, and may be used as starting point for more extensive simulations of polymer mechanics and fracture.

1. Introduction

Several recent advances in polymer science have concerned mechanochemistry, where the chemical response of chain molecules to mechanical stimuli is analyzed and exploited to produce new materials with enhanced toughness, as well as force-sensing and self-healing properties [1–4]. A good deal of activity in the area of polymer mechanochemistry has centered around the design of new mechanophores, which could be force-activated more efficiently and selectively [5–7]. These developments have often been guided by a combination of chemical intuition and rigorous quantum chemical calculations [8,9]. The classic problem of the scission of a plain hydrocarbon chain under tension may also be considered to be part this emerging field. Understanding the behavior of single polymer chains is an important prerequisite for explaining their ultimate mechanical properties. Chain scission is also crucially important for the mechanical properties of polymer interfaces, i.e. for adhesion [10,11].

The bulk mechanical properties of polymers depend on single-chain conformations and energetics, interchain interactions, viscous dissipation, entanglement density, as well as morphological features such as the presence of glassy or crystalline domains [12–14]. Models such as the Gaussian chain and Kratky-Porod models describe polymer elasticity and can be generalized to include bond deformation mechanisms, [15,16] while statistical fracture mechanics describes bulk failure using the weakest link hypothesis [17]. Due to its complexity, there is still no comprehensive model of polymer fracture at macroscopic scales, which incorporates also detailed molecular mechanisms [18]. Similar to other branches of polymer science, this will require statistical treatments [19] and seamless integration of models at different length scales [20]. Molecular dynamics (MD) simulations have and will certainly play an increasingly important role in this area, [21, 22] since they can be used to conduct computational experiments with complete atomic-scale knowledge about the state and evolution of a system [23]. However, in order to be comparable to experiments on real systems, they must be based on accurate interatomic potential energy functions that include the possibility of bond breaking and formation (reactive force fields) [24].

This study is a continuation of previous work by our group, where we simulated by MD the scission of single polyolefin chains (polyethylene, polypropylene and polystyrene) under tension [25]. In turn, this was motivated by the results of a critical analysis [26] of experimental data from single-molecule force spectroscopy (SMFS) [27], leading to new quantitative insights into the Lake-Thomas model for the fracture

☆ This article is part of a Special issue entitled: 'Bond Breaking in Polymers' published in Polymer.

* Corresponding author.
E-mail addresses: luca.liu@polimi.it (L. Liu), guido.raos@polimi.it (G. Raos).
[1] Present address: Dipartimento di Meccanica, Politecnico di Milano, via G. La Masa 1, 20156, Milano, Italy.

https://doi.org/10.1016/j.polymer.2026.129732
Received 1 December 2025; Received in revised form 6 February 2026; Accepted 9 February 2026
Available online 10 February 2026

of rubber networks [28]. There, the work of scission per main chain bond (U) was estimated to be of the order of 60 kJ/mol for typical hydrocarbon chains. Note that this is much lower than the thermal dissociation energy of C–C single bonds (about 350 kJ/mol) [29]. We point out that also this "experimental" value is subject to some uncertainty, originating mainly from the difficulty of controlling chain length and measuring end-to-end distances accurately in SMFS. In our simulations, [25] we obtained $U \simeq$ 20–45 kJ/mol, depending on the stereochemistry of the chains (we found that the isotactic polymers were systematically tougher than the others) and on the effective viscosity of the surrounding medium. Thus, while the experiments and the simulations agree on the order of magnitude of the Lake-Thomas parameter U, there is still a 50% difference between them. One possible source of this discrepancy is the force field that was used in those simulations (ci-ReaxFF) [30]. The aim of this work is to test its reliability, by comparing it with other reactive force fields and *ab initio* calculations.

Here present a combination of reactive MD and quantum chemical calculations. Four reactive force fields, namely AIREBO [31], MEAM [32], ReaxFF [33] and ci-ReaxFF [30], were employed to model deformation and bond scission during mechanical loading. These force fields enable the simulation of large systems by MD, capturing essential features of molecular interactions and thermal motion. Quantum chemical methods, in particular Density Functional Theory (DFT), were used as a benchmark to evaluate the accuracy of results obtained from these classical reactive force fields.

Two types of simulations were performed. First, room-temperature MD simulations were conducted on a polyethylene-like chain with 202 carbon atoms ($C_{202}H_{406}$, henceforth C202 for short), subject to elongation at constant velocity until breakup. Second, DFT-based energy minimization under a tensile force were performed on shorter *n*-hexadecane chain ($C_{16}H_{34}$, henceforth C16). The quantum chemical results were compared with the force field calculations on the same C16 chain. This dual approach provides a comprehensive understanding of the strengths and limitations of reactive force fields for simulating polymer mechanics at different scales.

The next section provides further details about the computational procedures. Next, we present first the results on C202, and then those on C16. The final section summarizes our conclusions.

2. Methods and models

2.1. Force fields

To model interatomic interactions, four different reactive force fields were employed. Each of these represents a different approach to describe internal deformation of the molecules, bond breaking and non-bonded interactions. In general they have different accuracies, depending also on the chemical composition of the system, and different computational costs [34].

AIREBO potential. AIREBO is an acronym for Adaptive Intermolecular Reactive Bond Order potential [31]. It was designed for hydrocarbons and includes three primary interaction terms:

$$E_{\mathrm{AIREBO}} = E_{\mathrm{REBO}} + E_{\mathrm{LJ}} + E_{\mathrm{torsion}}, \tag{1}$$

where:

- E_{REBO}: Reactive Empirical Bond Order term, [35] which models covalent bond interactions through a bond-order formulation, allowing dynamic bond breaking and formation.
- E_{LJ}: Van der Waals interaction term, implemented via a modified Lennard-Jones potential to account for non-bonded dispersive and repulsive forces.
- E_{torsion}: Torsional interaction term, capturing out-of-plane deformations to describe rotational energy barriers around bonds.

AIREBO is computationally efficient and widely used for hydrocarbon systems, but lacks explicit angular terms and electrostatic interactions. The latter are usually small for hydrocarbons, given the similar electronegativities of C and H that would result in near-zero atomic charges.

MEAM potential. The Modified Embedded-Atom Method (MEAM) [32] is an extension of the Embedded-Atom Method (EAM), [36] which was originally developed for metallic systems. MEAM improves upon EAM by introducing angle-dependent interactions among the atoms, making it more suitable for materials with directional bonding.

The total energy in MEAM is given by:

$$E_{\mathrm{MEAM}} = \sum_i \left[F(\bar{\rho}_i) + \frac{1}{2} \sum_{j \neq i} S_{ij} \phi(R_{ij}) \right], \tag{2}$$

where:

- $F(\bar{\rho}_i)$: Embedding function, which incorporates the effect of a local atomic electron density at an atom ($\bar{\rho}_i$) coming from neighboring atoms, to determine it contribution to the total energy. The electron densities are spherically symmetric in EAM, but they have an angular dependence in MEAM.
- $S_{ij}\phi(R_{ij})$: Pairwise term depending on the interatomic distance R_{ij}, representing both bonding (covalent) and non-bonding (Van der Waals) interactions among these atoms.

A version of MEAM was specifically parametrized for saturated hydrocarbons, [32] so in principle it should be applicable also to polyethylene. It has not been extensively adopted, but one of its early applications concerned the fracture of short hydrocarbon chains [37].

ReaxFF potential. The Reactive Force Field (ReaxFF) is an empirical potential based on the concept of bond order. The bond orders between neighboring atoms are dynamically adjusted at every step of a simulation and determine their interaction. The total energy in ReaxFF is given by:

$$E_{\mathrm{ReaxFF}} = E_{\mathrm{bond}} + E_{\mathrm{over}} + E_{\mathrm{under}} + E_{\mathrm{lp}} + E_{\mathrm{val}} + E_{\mathrm{tor}} + E_{\mathrm{vdW}} + E_{\mathrm{Coul}}, \tag{3}$$

where:

- E_{bond}: accounts for bond stretching and breaking.
- E_{over} and E_{under}: penalizes over-coordination and under-coordination of atoms.
- E_{lp}, E_{val}, and E_{tor}: describes lone pair, valence angle, and torsional contributions.
- E_{vdW} and E_{Coul}: incorporate van der Waals and electrostatic interactions, with charge equilibration performed at every timestep.

ReaxFF is highly flexible and captures bond formation and dissociation accurately, potentially making it one of the most interesting force fields for mechanochemistry. On the down side, we shall see that it is the most costly force field among those tested here. Note that there are several parametrizations of ReaxFF, depending of the chemistry of the system being studied [38]. We have used the gas-phase version for C, H and O, which is applicable also to combustion reactions [33,39].

ci-ReaxFF potential. The charge-implicit Reactive Force Field (ci-ReaxFF) is a variant of ReaxFF that neglects all electrostatic interactions, embedding them in the remaining potential energy terms and eliminating the need for any charge equilibration [30]. From this point of view, it is similar to AIREBO and MEAM. This modification simplifies calculations and reduces the computational cost, while preserving most of the essential features of ReaxFF. The total energy is expressed as:

$$E_{\mathrm{ci\text{-}ReaxFF}} = E_{\mathrm{bond}} + E_{\mathrm{over}} + E_{\mathrm{under}} + E_{\mathrm{lp}} + E_{\mathrm{val}} + E_{\mathrm{tor}} + E_{\mathrm{vdW}}. \tag{4}$$

The parameters of the terms that are retained have been re-optimized, to compensate for the absence of Coulomb interactions.

2.2. Molecular dynamics

The tensile failure of C202 was simulated by MD with the LAMMPS code, [40] following the general methodology of our previous work [25].

The motion of the atoms was described by the Langevin equation:

$$m_i \frac{d^2\mathbf{r}_i}{dt^2} = -\nabla_i E_{FF} - \gamma \frac{d\mathbf{r}_i}{dt} + \mathbf{X}(t) \qquad (i = 1, \ldots, N), \tag{5}$$

where m_i is the mass of atom i, $\mathbf{r}_i$ is its position, $-\nabla_i E_{FF}$ is the force on it as computed from the selected force field, γ is a friction coefficient, and $\mathbf{X}(t)$ is a stochastic force drawn from a normal distribution. This distribution has a variance that is proportional to the system's temperature and is inversely proportional to the friction coefficient. Together, the friction and random forces make up the so-called Langevin thermostat [23]. The thermostat has an important role in MD simulation, especially under non-equilibrium conditions such as in this case. The friction coefficient γ may be related to the viscosity of the surrounding (implicit) solvent, and we showed that it can have an effect on the outcome of the simulations. Here we used the value γ=0.01 fs^{-1} that corresponds to typical low-viscosity, low-molecular-weight hydrocarbons [25].

A model of a C202 chain was generated in a stretched conformation and equilibrated using the Langevin thermostat at 300 K for 5 ns. Next, each polymer chain was gently brought to an end-to-end distance of $R_{ee}(0) = 20$ nm and equilibrated for another 5 ns while maintaining this distance fixed. Note that $R_{ee}(0)$ is substantially larger than the unperturbed end-to-end distance of the polymer (6–7 nm), yet it remains well below the fully extended contour length (25.6 nm).

The previous equilibration step provided 200 starting configurations for an equal number of tensile loading simulations. The terminal carbon atoms were pulled apart at a velocity of $v = 2.5$ m/s in opposite directions. The pulling process continued until the polymer reached an end-to-end distance slightly beyond the failure point, stopping a few angstroms after chain scission to capture the complete failure behavior. The total energy and the forces on the terminal atoms were recorded, averaged and then plotted as a function of the end-to-end distance of the chain.

The timestep varied according to the force field: 0.5 fs for AIREBO, 0.1 fs for MEAM, and 0.25 fs for ReaxFF and ci-ReaxFF. In our experience, the adoption of longer timesteps could lead to inaccuracies or even failure of the simulations.

2.2.1. Ab initio calculations

The DFT calculations were performed with the ORCA 6.0 code [41,42]. We used the B3LYP functional [43,44] in combination with the def2-SVP basis set [45], with an auxiliary basis set to fit Coulomb and exchange interactions [46,47]. Grimme's D3BJ correction was included to model dispersion effects, which are not accounted for by B3LYP [48,49]. We tested both the restricted and unrestricted versions of the Kohn–Sham equations so as to check the possible effect of unpaired electrons on chain stretching and breaking, which however was found to be negligible.

The geometry of the molecule was first fully optimized in the zig-zag, trans-planar conformation. Afterwards, several optimizations were performed for progressively increasing values of an external force, applied to the terminal carbons [8]. This corresponds to the "external force is explicitly included" (EFEI) approach to modeling mechanochemical processes. Each new calculation produced a minimum with a increasing end-to-end distance, up to a critical value of the force where one C–C bonds breaks. When this occurs the geometry optimization does not converge any more, as the end-to-end distance increases indefinitely. Analogous calculations were performed also with LAMMPS, for each reactive force field. Contrary to the simulations on the long chains, they did not involve molecular dynamics or hard constraints on the end-to-end distance. Instead, we applied the external force quasi-statically in incremental steps and performed an energy minimization after each step to relax the geometry.

These geometry optimizations obviously neglect the effects of thermal motion. For ease of comparison with the MD simulations, also the results from these calculations will plotted with the end-to-end distance on the horizontal axis, even though this is a dependent variable in this case.

3. Results and discussions

The central problem of this article is the dependence of the mechanical response of a single polyethylene (PE) chain on the reactive force field used to model it. We will first discuss the MD simulations of the C202 chain, and then examine the results for the C16 chain. Images of the molecules the accompany our discussion were generated using the VMD program [50].

3.1. C202 simulations

3.1.1. Energy versus end-to-end distance

The total energy of a polymer chain depends on its state of deformation. Fig. 1 shows this quantity across the four force fields, highlighting distinct trends in their description of polymer elasticity and failure. These plots were obtained by superposing the data from 200 independent trajectories, and subtracting the average energies at the stating point [$R_{ee}(0) = 20$ nm] in order to have a common reference value across all simulations. Despite of this, the scales of the energies reported on the vertical axes can be very different, reflecting important differences between the force fields. Note also that, while the total energy is the sum of the potential energy (from the force field) and kinetic energy of the atoms, the latter is constant on average, thanks to the action of the MD thermostat. Therefore it cancels out when computing energy differences, and a plot of the total energy would be virtually undistinguishable from that of the potential energy.

The energy profiles highlight three or four distinct stages of deformation. For the AIREBO force field (Fig. 1, top-left panel) we have:

I. Entropic regime (up to 260 Å): Here the total energy remains nearly constant as the polymer chain is in a relaxed state, with limited resistance to deformation. The polymer gradually transitions from a disordered coiled conformation (see Fig. 2a) to an extended zig-zag conformation (see Fig. 2b).
II. Enthalpic regime:
   (a) (260–340 Å): As the polymer undergoes further stretching, the total energy suddenly rises in a parabolic manner due to the onset of bond stretching and angle bending.
   (b) (340–354 Å): The energy continues to increase, but at a different rate, as bond angles oscillate around 180° and bond stretching dominates (see Fig. 2c, Fig. 5a and Fig. 6a). We call this pre-failure regime.
III. Post-failure regime (beyond 354 Å): after failure of one bond, we have two separate fragments, which relax back to a random-coil conformation while they are dragged away from each other. The elastic energy stored in the chain up to the breaking point is dissipated as heat.

According Fig. 1, for all the other force fields chain scissions occurs within a broad range of end-to-end distances—roughly between 280 and 310 Å—but always well below those that characterize AIREBO. Fig. 3 shows the C202 configurations immediately before scission, for each of the force fields. It is evident that only AIREBO predicts the possibility to reach a fully stretched, collinear chain conformation. This seems incompatible with common ideas about the possible hybridization states of carbon, suggesting that failure should occur when the bond angles are still far from 180°. This is confirmed by the DFT results,

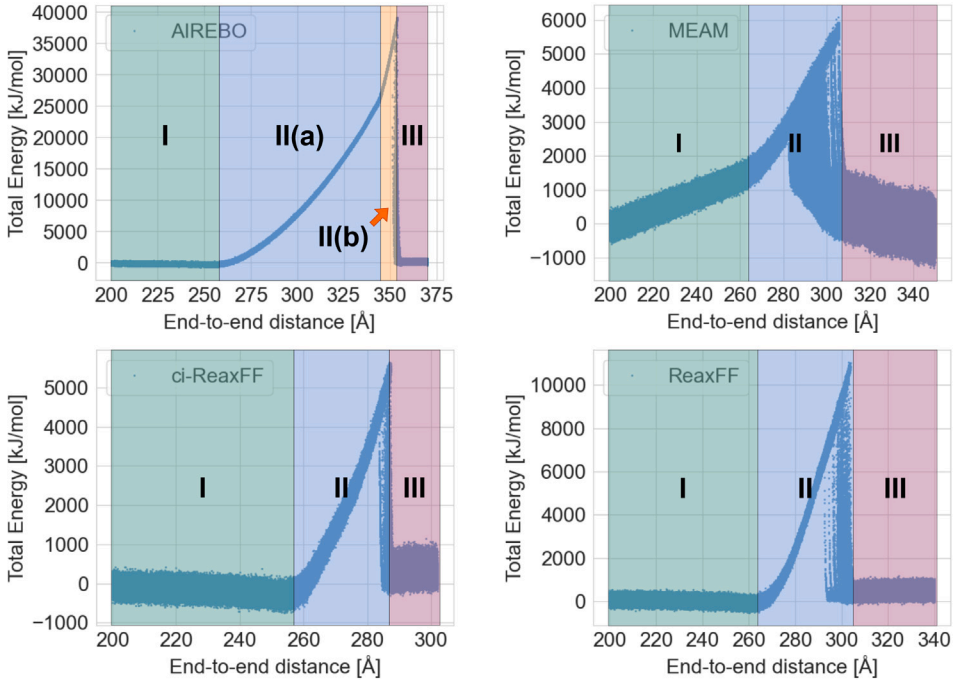

Fig. 1. Change in total energy versus end-to-end distance for C202, using different force fields. Clockwise, starting from the top-left corner: AIREBO, MEAM, ReaxFF, ci-ReaxFF.

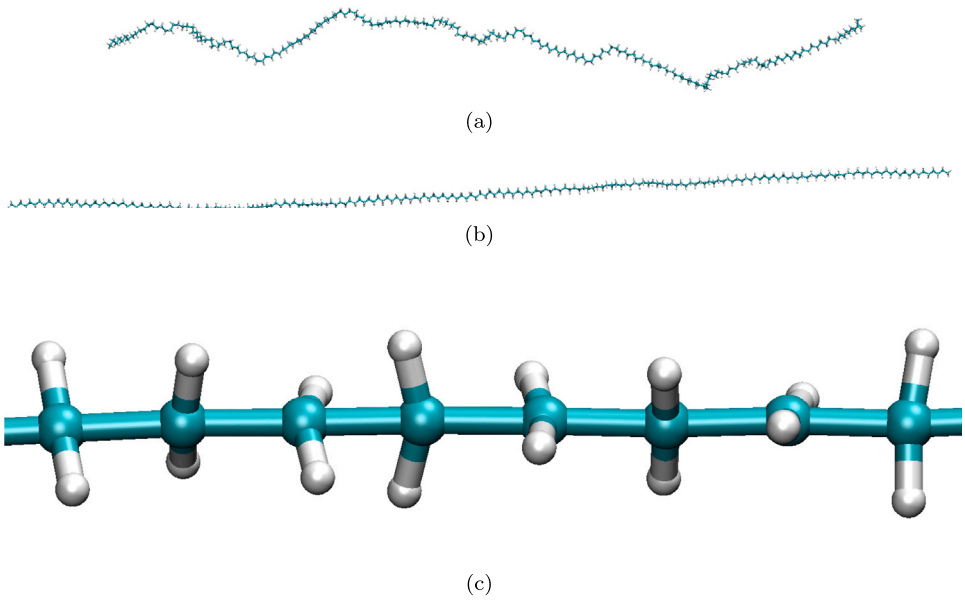

Fig. 2. Stages of polymer pulling according to the AIREBO force field: (a) relaxed state at the start of a simulation, (b) aligned under tension in the zig-zag conformation, and (c) section of a fully stretched chain immediately before failure.

which will be discussed later, where the average bond angle at failure is approximately 130°. Thus, the pre-failure regime appears to be a specific artifact of the AIREBO force field. For the same reasons, also the very high value of the total energy at failure is probably unrealistic. Note also that the AIREBO curve appears to be narrower than for the other force fields, apparently indicating less spread in the energies from independent simulations, because the overall energy scale is so much larger.

The energy profile for the MEAM model (Fig. 1b) displays only three stages (entropic, enthalpic, and post-scission). Note also that there are large energy variations during both the initial stretching phase and the post-failure dragging of chain fragments. These features are unexpected and somewhat puzzling: the energy variation from a curved chain to an extended zig-zag chain should not be significant compared to the energy variation in the enthalpic stretching phase (the second stage), and the same applies to the post-breakup phase. Finally, in the MEAM simulations there is a large statistical scatter of the end-to-end distances at failure, as measured by the width of the vertical section of the plots. This contrasts with AIREBO, where the chains always reach very similar end-to-end distances before failing.

Examining the energy plots for ReaxFF and ci-ReaxFF (Fig. 1c,d), we observe that both force fields avoid the unrealistic features seen in AIREBO and MEAM. Unlike AIREBO they do not exhibit the pre-failure regime, and unlike MEAM they do not show excessive energy variations

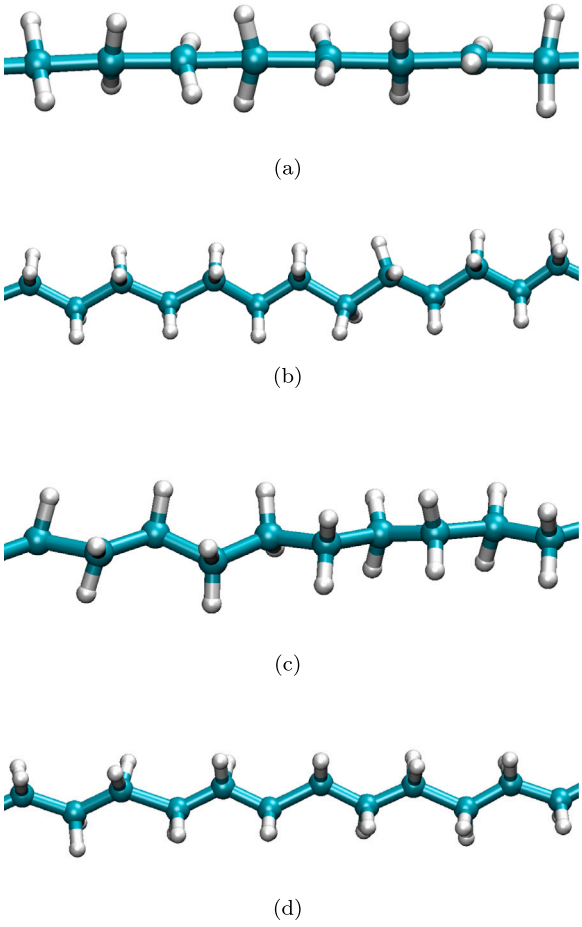

Fig. 3. Sections of a C202 chain immediately before scission: (a) AIREBO, (b) MEAM, (c) ci-ReaxFF, (d) ReaxFF.

in the entropic and post-failure regimes. Interestingly, the energy at breakup of ci-ReaxFF is actually closer to MEAM than to ReaxFF. However, now the overall energy change is almost entirely confined to the final enthalpic step. The scatter in the end-to-end distances at failure is similar and intermediate between AIREBO and MEAM.

In conclusion, there are major differences as well as some similarities among the force fields. It is difficult to pin down exactly the origin of these features, given their complicated functional forms. Judging solely from the shape of the energy curves, ReaxFF and ci-ReaxFF seems to provide a more reasonable representation of polymer deformation and failure, while AIREBO and MEAM introduce some artifacts that might limit their predictive accuracy.

3.1.2. Force versus end-to-end distance

The force–elongation curves offer a complementary perspective on the mechanical properties of a single polymer chain. Unlike the total energy, forces are measurable by SMFS [27] and they are more directly relevant for mechanochemical behavior [2]. The force experienced by a chain under tension is a function of the end-to-end distance (R_{ee}) that is expected to increase monotonically, first slowly (entropic elasticity) and then much more steeply (enthalpic elasticity), up to the failure point (R^*_{ee}) where it drops suddenly to zero. In our simulations, this quantity is obtained by recording the forces on the terminal atoms (these are computed at every step of an MD simulation, for all the atoms), projecting them along the end-to-end distance, and taking their difference to obtain the net force on the chain. Next, these forces are also averaged over all chains and over a limited time window (corresponding to a small range of values for the end-to-end distance), to eliminate atomic-scale fluctuations and allow general trends to stand out more clearly [25].

The integral of the force versus elongation curves provides the work of chain fracture:

$$W = \int_{R_{ee}(0)}^{R^*_{ee}} F(R_{ee})\, d R_{ee} \,. \tag{6}$$

Unlike the chain's total energy, that was discussed at the previous point, the work of fracture includes the effect of energy dissipation, which is connected to viscoelastic properties of the chain and its environment (represented here by the Langevin thermostat). Viscous dissipation is expected to play an important role in our simulations, considering that the chains are deformed at a very high rate, and therefore the process is far from being reversible.

Fig. 4 summarizes our results for the forces and the work of fracture. Some of the trends that emerged from the analysis of the energies are evident also in these plots. The AIREBO model deforms according to a three stage process, unlike the others that have only two. The force at breakup of AIREBO is also much larger than the others. The MEAM model has the poorest mechanical properties, but it displays an anomalous growth of the force already in the entropic domain. Indeed, in MEAM there is not a clear-cut difference between the enthalpic and entropic regimes. The ReaxFF and ci-ReaxFF curves are in between. The latter is very similar to that reported in our previous publication [25].

3.1.3. Bond length and bond angle distributions

The evolution of the bond lengths and bond angles offers interesting insights into the atomic-level mechanisms of chain deformation. Figs. 5 and 6 present two-dimensional heatmaps of their distributions as a function of the end-to-end distance.

Intuitively, one would expect little or not change in these internal degrees of freedom up to the onset of enthalpic elasticity, when the chain is in the zig-zag trans-planar conformation but still far from its breaking point. Indeed, both lengths and angles are almost unchanged up to about 250 Å (or more). Afterwards, a further elongation could only be achieved by an increase of the C–C bonds lengths, an opening of the C–C-C angles, or any combination of these. In this respect, we see some further differences among the force fields. According to AIREBO, the bonds lengths change concurrently with the angles, implying that they have comparable stiffnesses. The plot of the bonds length has some "kinks" and sudden changes in slope, which do not have a clear physical or chemical interpretation. ReaxFF and ci-ReaxFF even have near-discontinuities in the bond length that occur before breakup, which also seem to be an unphysical result of the parametrization. The MEAM model is characterized by comparable changes of both bond lengths and angles.

3.1.4. Comparison of force field performance and cost

Table 1 summarizes some key structural and mechanical properties derived from simulations using various force fields. While the relaxed molecular structures (bond length and bond angle) are fairly consistent across all force fields, notable differences emerge in their ultimate mechanical properties. These are the maximum force at failure, the end-to-end distance at failure, and the energy characteristics. Here we assess the accuracy of these results by comparing them with the experimental findings. Later on we will also use the DFT calculations as a benchmark.

A key quantity that can be used for comparison is the work required to break the polymer chain. Following the approach of Lake and Thomas [28], we may divide the work of failure W [see again Eq. (6)] by the number of chain bonds ($n = 201$ in our case):

$$W = nU \,. \tag{7}$$

This yields U, the energy per bond at failure, which has been estimated to be approximately 60 kJ/mol for hydrocarbon polymers [26]. Our simulated values are reported in Table 1.

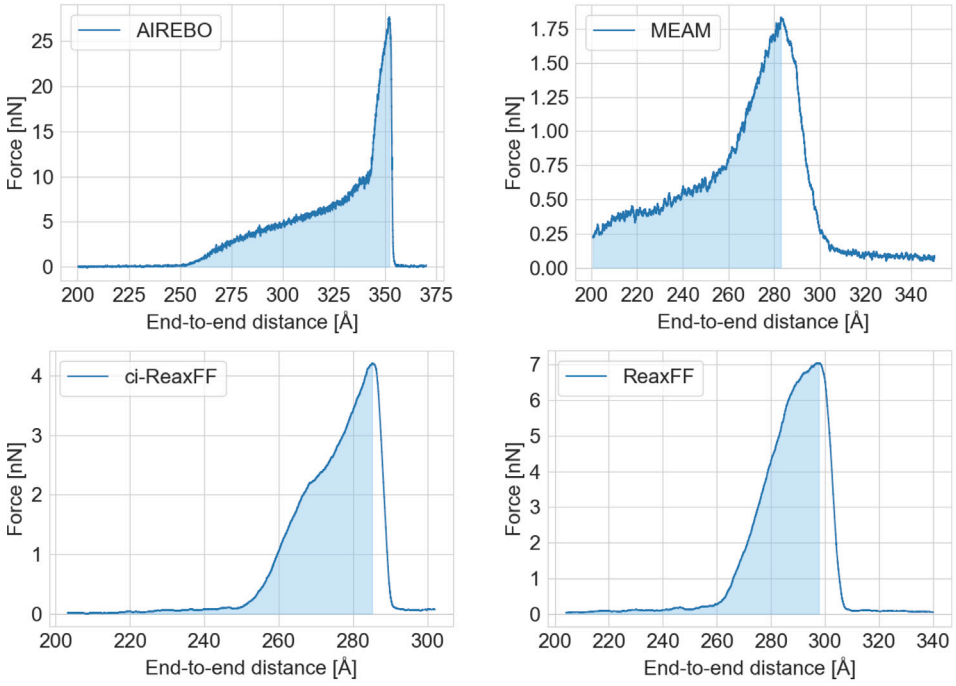

Fig. 4. Force versus end-to-end distance for C202 using different force fields. The shaded areas represent the work done to elongate and break the chains.

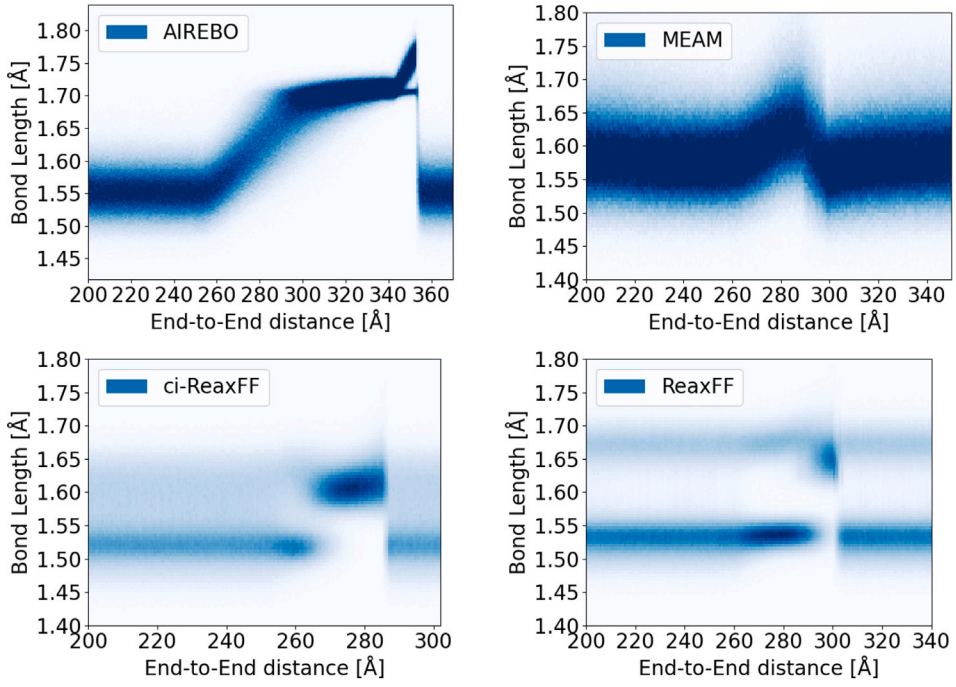

Fig. 5. Bond length distributions as a function of end-to-end distance for C202 according to different force fields.

Table 1
Comparison of mechanical properties for different force fields. Failure force, failure distance, and work of failure are average quantities. The last column U denotes the work of failure divided by the number of bonds.

Force field	Failure force [nN]	Failure distance [Å]	Work of failure [kJ/mol]	Max energy change [kJ/mol]	Min energy change [kJ/mol]	U [kJ/mol]
AIREBO	27.69	352.0	36,548	39,127	35,933	181.83
MEAM	1.83	282.9	3482	6080	2468	17.32
ci-ReaxFF	4.21	285.2	4303	5647	3927	21.41
ReaxFF	7.04	297.7	9186	11,039	6017	45.70

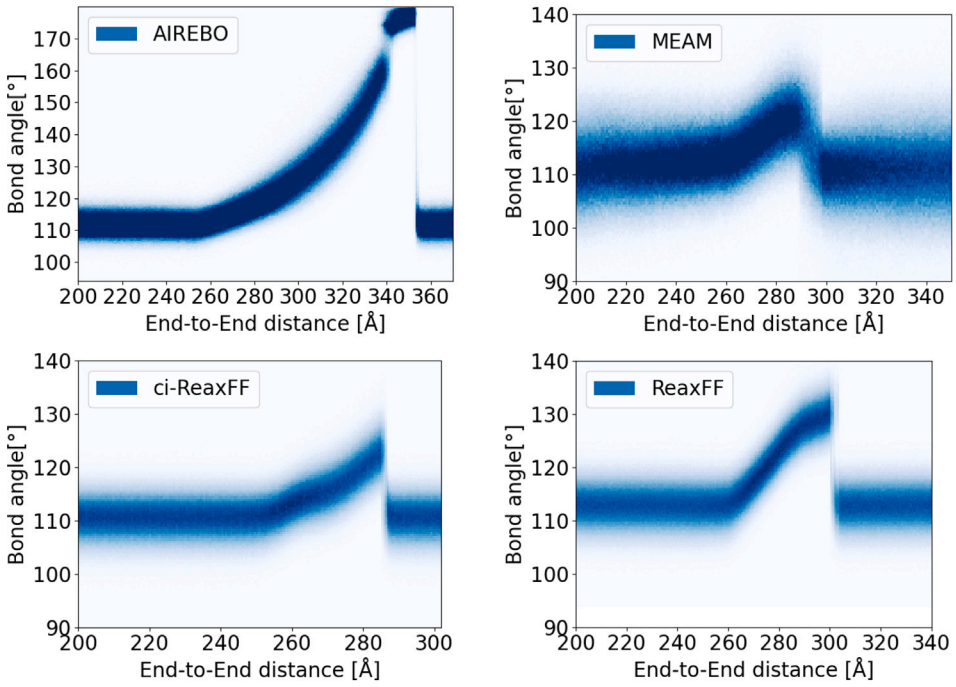

Fig. 6. Bond angle distributions as a function of end-to-end distance for C202 according to different force fields.

From this analysis, ReaxFF is closest to the experimental value of U. Based on the trends from our previous simulations, [25] a ReaxFF-based simulation of other polyolefins (e.g., polystyrene and polypropylene) or with higher background friction would further increase the value of U, bringing it even closer to the experimental value. Therefore, this appears to be a reliable force field for predicting single-chain mechanical properties.

AIREBO significantly overestimates the failure force and work done. Additionally, its bond scission mechanism is activated only at extreme deformations, allowing all bond angles to fully open (see again Fig. 2c) before any of the 201 bonds reaches its breaking threshold. This results in an unrealistic mechanical response, as it prevents the gradual accumulation of bond strain and fails to capture progressive bond weakening due to collective deformation. Consequently, the polymer chain undergoes excessive stretching before failure, leading to an overestimation of the maximum elongation, of the failure force and of the total work required for rupture.

MEAM, on the other hand, underestimates both the failure force and the work done. Differences with the other force fields are likely due to its very different mathematical formulation and parametrization. Unlike other force fields, MEAM does not include explicit terms for covalent bonding, van der Waals interactions, or torsional contributions. Instead, all interactions are embedded within a non-additive, pairwise potential, in a way which may not be perfectly balanced. As a result, MEAM struggles to capture accurately the transition from the entropic to elasticity and bond breaking, making it unsuitable for modeling polymer mechanics.

Also ci-ReaxFF underestimates the failure properties compared to ReaxFF, but to a smaller extent. We have already pointed out that their energy–elongation and force–elongation curves are more similar than those of the other models. This is consistent with the fact that they share the same functional form, with the exception of electrostatic interactions.

Although the U value obtained with ci-ReaxFF is numerically closer to MEAM than to ReaxFF, their underlying failure mechanisms are very different. In particular, MEAM shows an anomalously high initial resistance to deformation. This can plausibly be linked to MEAM's explicit dependence of the energy on the local atomic (electron) density, which does not seem to provide a clear-cut, quantitative distinction between bonded and non-bonded contributions to the energy.

Table 2
Comparison of the computational cost of different force fields.

Force field	Cost (CPU hours/ns)	Timestep (fs)
AIREBO	1.61	0.5
MEAM	6.87	0.1
ci-ReaxFF	6.51	0.25
ReaxFF	8.51	0.25

Before closing this section, we compare the computational cost of the force fields [34]. This is an important aspect for any MD simulation, because its accuracy depends not only on the quality of the force field, but also on the possibility to sample adequately the phase space and obtain reliable averages by running long simulations on large systems. Table 2 shows that there is up to a five-fold difference in the cost of the models. All timings were obtained on a workstation with an Intel Core i5-9300H CPU (2.40 GHz). AIREBO is the least demanding method, also because it is compatible with a relatively large timestep. ReaxFF is the most expensive method, as expected. ci-ReaxFF is cheaper, but only by a relatively modest 15%. The difference might be larger for larger systems, in articular in combination with periodic boundary conditions, due to the cost of dealing with long-range interactions by Ewald summations and related methods [23]. The cost of MEAM is also fairly large, despite of the use of a relatively simple functional form, because it requires a very small integration timestep.

3.2. C16 simulations

We now switch to the results for a shorter polyethylene-like chain (C16), which allow us to clarify how well the force fields align with

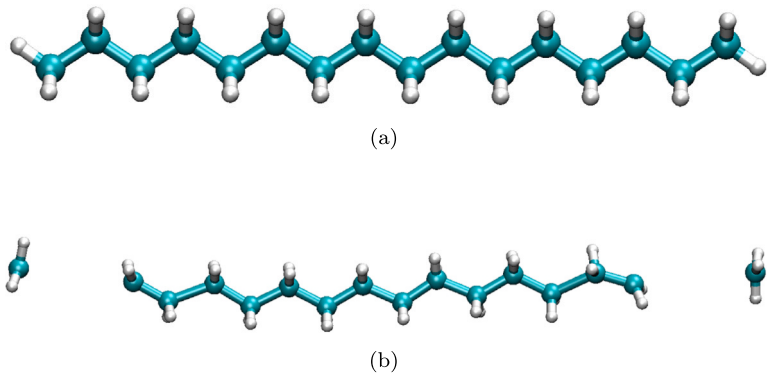

Fig. 7. Initial geometry (a) and geometry after breakup (b) from DFT calculations on hexadecane.

first-principles DFT calculations of force-induced deformation and failure. These calculations started from a planar zig-zag conformation and, re-optimizing its geometry subject to a gradually increasing force, eventually produced scission of the two external bonds, as shown in Fig. 7.

Fig. 8 shows the force and the energy versus the end-to-end distance from DFT the calculations, highlighting the mechanical response of C16 under stretching. The curves start from the trans-planar conformation and terminate at the last stable minimum, before breakup. The force is linear up to about 20 Å, corresponding to a 5% elongation. Afterwards the force gradually levels off up to a threshold of about 6.1 nN, beyond which the bonds break and the geometry optimization no longer converges. The total energy change at breakup equals the integral of the force–distance curve (there is no energy dissipation in this case) and its value is 870.3 kJ/mol. Hence, a hexadecane chain can store a mechanical energy which is two to three times the energy required to break a C–C single bond, but does not undergo scission because this energy is spread across several bonds. Dividing this energy by the number of bonds ($n = 15$), we obtain $U = 58.02$ kJ/mol, apparently in perfect agreement with the estimate by Wang et al. [26]. Note however that the present result was obtained by static energy minimizations, neglecting the effects of thermal motion, viscous dissipation and torsional barriers (the chain started from a trans-planar conformation).

Fig. 9 shows histograms of the bond lengths and bond angles, collected across all deformation states but distinguishing according to their ID so as to highlight possible heterogeneities in the deformation. Indeed, the plots show that the terminals of the chain experience a significantly different deformation history compared to the internal ones. The deformation has a left–right symmetry, as it should. It affects all parts of the chain, but tends to concentrate at the two ends. Just before scission, the C–C bond lengths are about 1.85 Å at the terminals, while they are 1.72 Å in the remainder of the chain (to be compared with 1.54 Å before deformation). Similarly, the two outermost angles are 135 °, while they are only 125 ° in the rest of the chain (about 112 ° before deformation). All this agrees with the fact that, within this model, scission occurs simultaneously at the two terminals, instead of a random bond in the middle of the chain.

We may now compare the DFT results with those obtained with LAMMPS using different force fields. Fig. 10 shows the results for AIREBO. Symmetry can be observed in both plots, as expected. However, unlike in the DFT calculations, the deformation of the terminal bonds and bond angles is comparable to that of the internal ones. All bond angles tend toward 180 ° as the chain approaches the failure point, resulting in a fully linear configuration (see Fig. 2c). All the bonds stretch up to 1.80 Å before breakup, but the density of the histograms around 1.70 Å indicates that there is an intermediate state

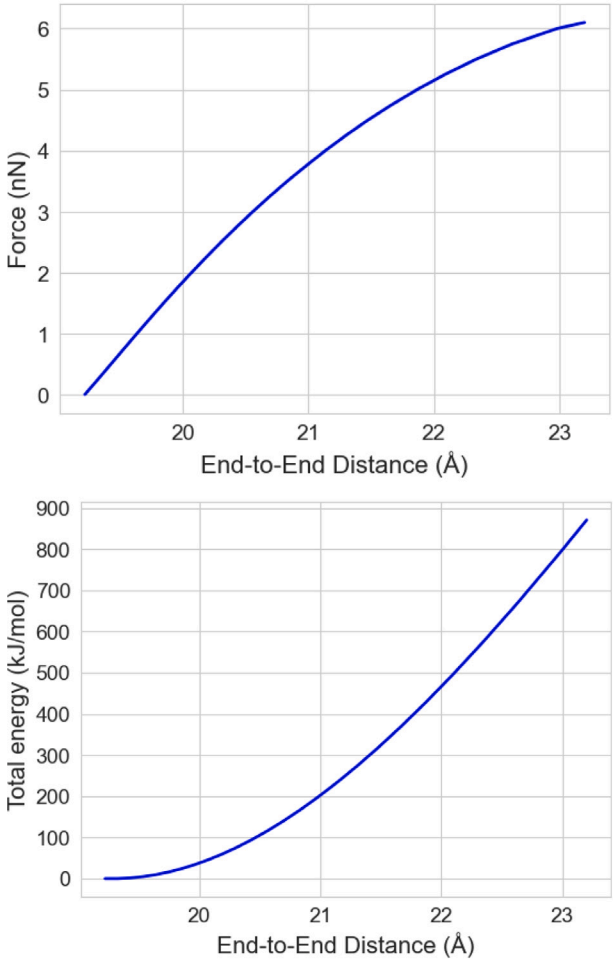

Fig. 8. DFT results (B3LYP-D3BJ/def2-SVP) for stretched hexadecane: force (above) and total energy (below) versus end-to-end distance.

of deformation where this is the preferred bond length. This is clearly an artifact of the AIREBO parametrization, which was observed also in the MD simulations (see again Fig. 5).

Fig. 11 shows that the chain deformation is very homogeneous also in the MEAM-based calculations. However the bonds can reach 2.9 Å and, at a later stage of deformation, also the bond angles become collinear. As a result, the chain stretches to unrealistically large values

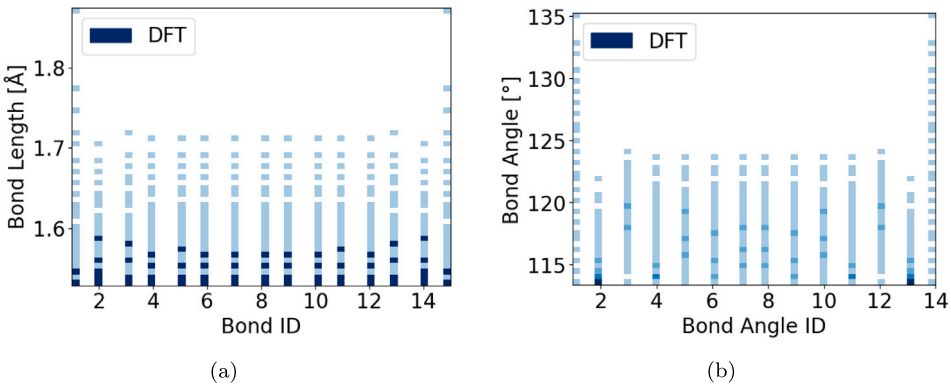

Fig. 9. Histograms showing the deformation of hexadecane in static DFT simulations: (a) Bond length vs. bond ID, and (b) Bond angle vs. bond angle ID.

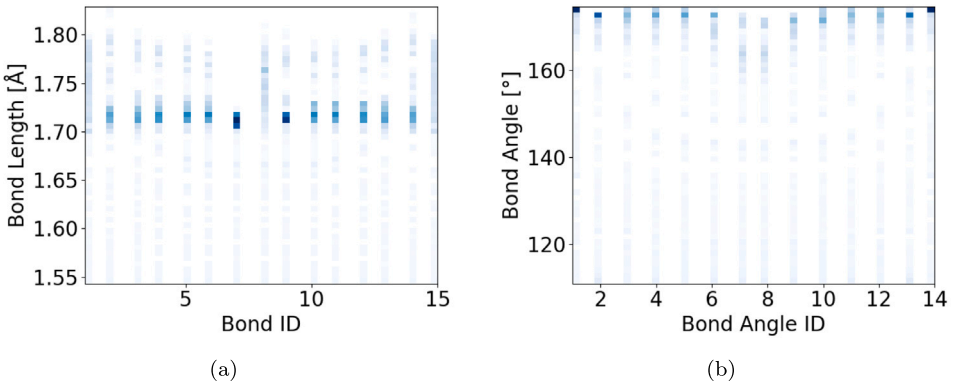

Fig. 10. Histograms showing the deformation of hexadecane in static AIREBO-based simulations: (a) Bond length vs. bond ID, and (b) Bond angle vs. bond angle ID.

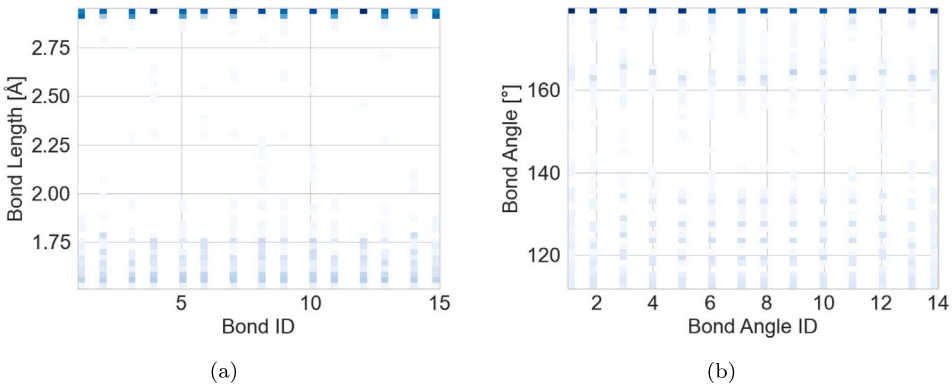

Fig. 11. Histograms showing the deformation of hexadecane in static MEAM-based simulations: (a) Bond length vs. bond ID, and (b) Bond angle vs. bond angle ID.

before snapping (about 44 Å). Interestingly, in the MD simulations MEAM predicted scission to occur earlier than any other model. Thus, there is a remarkable difference between the behavior of the MEAM model in MD simulations and the static energy minimizations. In any case, MEAM appears to be unsuitable for modeling the mechanics of saturated hydrocarbon chains.

Fig. 12 shows that the deformation mechanism of ci-ReaxFF is rather similar to that from the DFT calculations. The largest deformations tend to occur at the chain terminals. In the interior of the chain, bond length remain close to 1.60 Å and the angles reach about 125 °.

Finally, Fig. 13 illustrates the results from the ReaxFF-based calculations. The deformation of the bond lengths is remarkably heterogeneous, but it retains the expected left–right symmetry. Also, the bond lengths always remain within a reasonable range of values. The deformation of the bond angles is larger but similar to the DFT and ci-ReaxFF ones.

Table 3 presents a comparison of key properties characterizing the models. AIREBO and MEAM show significant deviations from the DFT predictions, while both ci-ReaxFF and ReaxFF compare favorably with it. A direct comparison of the deformation energies from DFT,

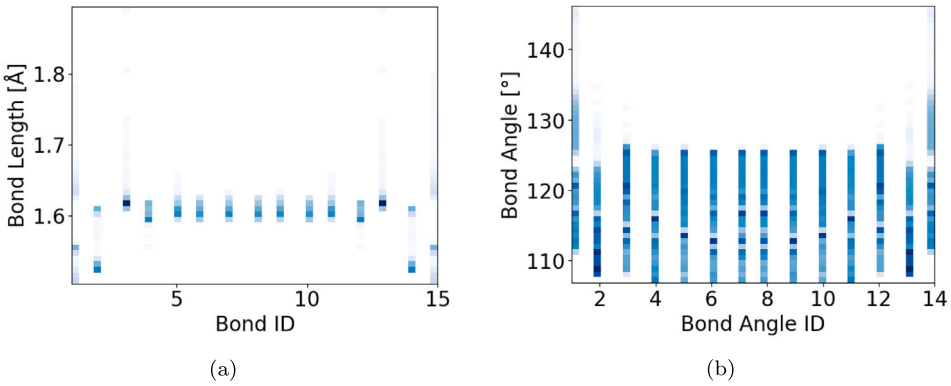

Fig. 12. Histograms showing the deformation of hexadecane in static ci-ReaxFF-based simulations: (a) Bond length vs. bond ID, and (b) Bond angle vs. bond angle ID.

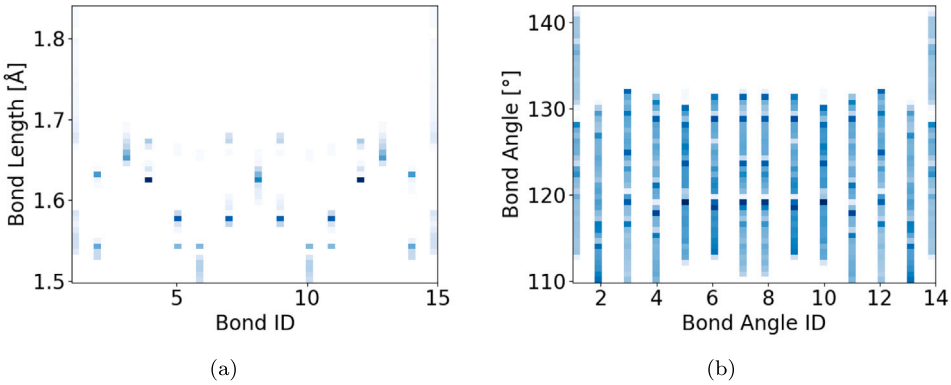

Fig. 13. Histograms showing the deformation of hexadecane in static ReaxFF-based simulations: (a) Bond length vs. bond ID, and (b) Bond angle vs. bond angle ID.

Table 3
Comparison of failure force, failure end-to-end distance, and energy characteristics for C16 across different models.

Model	Failure force [nN]	Failure end-to-end distance [Å]	Total energy change [kJ/mol]
AIREBO	36.92	26.8	3732.0
MEAM	7.85	44.1	3278.6
ci-ReaxFF	6.56	23.0	837.5
ReaxFF	8.77	23.2	955.2
DFT	6.10	23.2	870.3

ci-ReaxFF and ReaxFF is shown in Fig. 14. All curves terminate at their respective failure points. Overall, it highlights the close agreement between these reactive force fields and DFT, despite of the differences in their local deformation mechanisms.

4. Conclusions

In this study we have investigated the mechanical response of polyethylene-like chains under tensile loading using a combination of classical molecular dynamics and quantum chemical calculations. We have compared four reactive force fields—AIREBO, MEAM, ci-ReaxFF and ReaxFF—with DFT benchmark calculations, in order to assess their accuracy in describing the transition from entropic to enthalpic elasticity, local deformation mechanisms, energy evolution, and failure behavior.

Our results have revealed very significant differences in how these reactive force fields capture polymer stretching and failure. ReaxFF and ci-ReaxFF achieve the closest agreement with the quantum mechanochemical calculations. The work of fracture per chain bond predicted by them compares favorably with experimental estimates derived from the Lake-Thomas model, [26] confirming the findings of previous simulations conducted by our group with ci-ReaxFF [25]. In contrast, AIREBO seriously overestimates failure forces, deformation energy and maximum elongation. MEAM, on the other hand, underestimates these values in MD simulations, but behaves similarly to AIREBO in static energy minimization. The MEAM results, although quantitatively wrong, carry one important lesson for the computational screening of mechanophores. While static energy minimizations of short fragments are generally convenient and preferable due to their lower computational cost, there may situations where dynamical effects are important and would produce a completely different scenario.

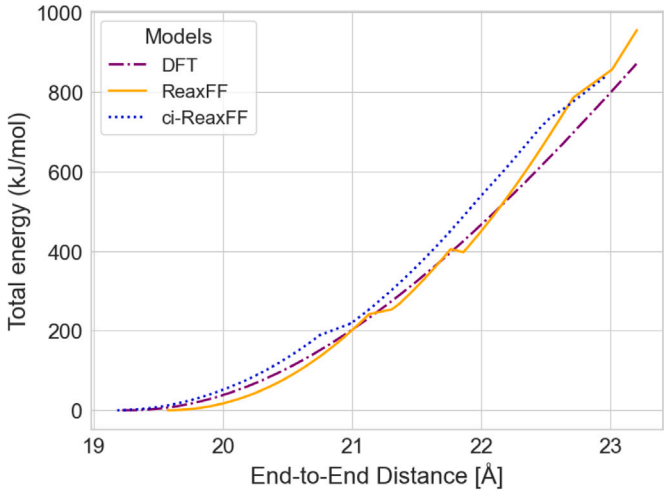

Fig. 14. Energy versus end-to-end distance for the C16 chain under mechanical stretching, comparing DFT (B3LYP-D3BJ/def2-SVP), ci-ReaxFF, and ReaxFF.

These should be modeled by MD, either *ab initio* or with a suitable force field.

Looking beyond single chains, our findings have broader implications for atomistic simulations of the mechanical properties of bulk polymers, where factors such as chain entanglements, crystallinity, and interchain interactions play a crucial role. The insights gained here lay the foundations for future simulations aimed at bridging molecular-scale behavior with the ultimate mechanical properties of polymer glasses and networks. Future work in this area may also include further improvements to the description of chain scission through the application of modern machine learning potentials [51].

CRediT authorship contribution statement

Luca Liu: Writing – original draft, Visualization, Investigation, Data curation. **Guido Raos:** Writing – review & editing, Supervision, Methodology, Funding acquisition, Conceptualization.

Declaration of competing interest

The authors declare that they have no known competing financial interests or personal relationships that could have appeared to influence the work reported in this paper.

Acknowledgment

Research by G.R. was supported by MIUR through the PRIN 2022 project "Protein adhesives for wet surfaces (PAWS)" (project code 2022YKWMT8–002).

Appendix. Supporting information

Sample LAMMPS input and output files from the MD simulations of C202 are freely available on Zenodo at the address: https://doi.org/10.5281/zenodo.17650058.

Data availability

Data are publicly available on Zenodo.

References

[1] C.J. Kloxin, T.F. Scott, B.J. Adzima, C.N. Bowman, Covalent adaptable networks (CANs): A unique paradigm in cross-linked polymers, Macromolecules 43 (6) (2010) 2643–2653, http://dx.doi.org/10.1021/ma902596s.
[2] L. Dong, L. Li, H. Chen, Y. Cao, H. Lei, Mechanochemistry: Fundamental principles and applications, Adv. Sci. (2024) http://dx.doi.org/10.1002/advs.202403949.
[3] Z. Shi, Y. Hu, X. Li, Polymer mechanochemistry in drug delivery: From controlled release to precise activation, J. Control. Release 365 (2024) 259–273, http://dx.doi.org/10.1016/j.jconrel.2023.10.042.
[4] Z.J. Wang, J.P. Gong, Mechanochemistry for on-demand polymer network materials, Macromolecules 58 (1) (2025) 4–17, http://dx.doi.org/10.1021/acs.macromol.4c02293.
[5] G. De Bo, Polymer mechanochemistry and the emergence of the mechanophore concept, Macromolecules 53 (18) (2020) 7615–7617, http://dx.doi.org/10.1021/acs.macromol.0c01683.
[6] Y. Sun, I. Kevlishvili, T.B. Kouznetsova, Z.P. Burke, S.L. Craig, H.J. Kulik, J.S. Moore, The tension-activated carbon–carbon bond, Chem 10 (10) (2024) 3055–3066, http://dx.doi.org/10.1016/j.chempr.2024.05.012.
[7] Z.J. Wang, S. Wang, J. Jiang, Y. Hu, T. Nakajima, S. Maeda, S.L. Craig, J.P. Gong, Effect of the activation force of mechanophore on its activation selectivity and efficiency in polymer networks, J. Am. Chem. Soc. 146 (19) (2024) 13336–13346, http://dx.doi.org/10.1021/jacs.4c01879.
[8] J. Ribas-Arino, D. Marx, Covalent mechanochemistry: Theoretical concepts and computational tools with applications to molecular nanomechanics, Chem. Rev. 112 (10) (2012) 5412–5487, http://dx.doi.org/10.1021/cr200399q.
[9] A. Germann, J. Meisner, Force-induced transition state rupture enables mechanistic control in aziridine mechanochemistry, Chem. Sci. 16 (45) (2025) 21454–21463, http://dx.doi.org/10.1039/D5SC04954G.
[10] G. Raos, B. Zappone, Polymer adhesion: Seeking new solutions for an old problem, Macromolecules 54 (23) (2021-12-14) 10617–10644, http://dx.doi.org/10.1021/acs.macromol.1c01182.
[11] G. Raos, B. Zappone, Tuning adhesion and energy dissipation in polymer films between solid surfaces via grafting and cross-linking, Macromolecules 57 (14) (2024) 6502–6513, http://dx.doi.org/10.1021/acs.macromol.4c00062.
[12] C. Creton, 50Th anniversary perspective: Networks and gels: Soft but dynamic and tough, Macromolecules 50 (21) (2017) 8297–8316, http://dx.doi.org/10.1021/acs.macromol.7b01698.
[13] J. Kim, G. Zhang, M. Shi, Z. Suo, Fracture, fatigue, and friction of polymers in which entanglements greatly outnumber cross-links, Science 374 (6564) (2021) 212–216, http://dx.doi.org/10.1126/science.abg6320.
[14] Z. Chen, Z. Suo, Thermodynamic and molecular origins of crack resistance in polymer networks, Chem. Rev. 126 (1) (2026) 606–670, http://dx.doi.org/10.1021/acs.chemrev.5c00663.
[15] S.R. Lavoie, R. Long, T. Tang, Modeling the mechanics of polymer chains with deformable and active bonds, J. Phys. Chem. B 124 (1) (2020) 253–265, http://dx.doi.org/10.1021/acs.jpcb.9b09068, PMID: 31790253.
[16] J. Zhu, L. Brassart, Stretching response of a polymer chain with deformable bonds, Phys. Rev. Lett. 134 (2025) 218101, http://dx.doi.org/10.1103/PhysRevLett.134.218101.
[17] S.B. Batdorf, H.L. Heinisch Jr., Weakest link theory reformulated for arbitrary fracture criterion, J. Am. Ceram. Soc. 61 (6-7) (1978) 355–358, http://dx.doi.org/10.1111/j.1151-2916.1978.tb09327.x.
[18] N. McCrum, C. Buckley, C. Bucknall, Principles of polymer engineering, in: Oxford science publications, Oxford University Press, 1997.
[19] M. Rubinstein, R.H. Colby, Polymer physics, Oxford university Press, Oxford, 2003.
[20] Z. Tang, W. Xian, J. He, R. Long, Y. Li, From bonds to breaks: multiscale perspectives on polymer network fracture, Int. J. Smart Nano Mater. 16 (4) (2025) 779–844, http://dx.doi.org/10.1080/19475411.2025.2582826.
[21] A. Baljon, M.O. Robbins, Simulations of crazing in polymer glasses: Effect of chain length and surface tension, Macromolecules 34 (12) (2001) 4200–4209, http://dx.doi.org/10.1021/ma0012393.
[22] T. Ge, F. Pierce, D. Perahia, G.S. Grest, M.O. Robbins, Molecular dynamics simulations of polymer welding: Strength from interfacial entanglements, Phys. Rev. Lett. 110 (9) (2013) 098301, http://dx.doi.org/10.1103/PhysRevLett.110.098301.
[23] M.P. Allen, D.J. Tildesley, Computer Simulation of Liquids, second ed., Oxford University Press, 2017.
[24] M.H. Müser, S.V. Sukhomlinov, L. Pastewka, Interatomic potentials: Achievements and challenges, Adv. Phys.: X 8 (1) (2023) 2093129, http://dx.doi.org/10.1080/23746149.2022.2093129.
[25] N. Fakhrayi Mofrad, P. Bahadori, G. Raos, Ultimate molecular mechanical properties of polyolefin chains, Macromolecules 57 (9) (2024) 3901–3913, http://dx.doi.org/10.1021/acs.macromol.3c02609.
[26] S. Wang, S. Panyukov, M. Rubinstein, S.L. Craig, Quantitative adjustment to the molecular energy parameter in the lake–Thomas theory of polymer fracture energy, Macromolecules 52 (7) (2019) 2772–2777, http://dx.doi.org/10.1021/acs.macromol.8b02341.

[27] W. Zhang, X. Zhang, Single molecule mechanochemistry of macromolecules, Prog. Polym. Sci. 28 (8) (2003) 1271–1295, http://dx.doi.org/10.1016/S0079-6700(03)00046-7.
[28] G.J. Lake, A.G. Thomas, The strength of highly elastic materials, Proc. R. Soc. Lond. Ser. A. Math. Phys. Sci. 300 (1460) (1967) 108–119, http://dx.doi.org/10.1098/rspa.1967.0160.
[29] L. Pauling, General Chemistry, Dover Publications, 1988.
[30] M. Kański, D. Maciazek, Z. Postawa, C.M. Ashraf, A.C. Van Duin, B.J. Garrison, Development of a charge-implicit reaxff potential for hydrocarbon systems, J. Phys. Chem. Lett. 9 (2) (2018) 359–363, http://dx.doi.org/10.1021/acs.jpclett.7b03155.
[31] S.J. Stuart, A.B. Tutein, J.A. Harrison, A reactive potential for hydrocarbons with intermolecular interactions, J. Chem. Phys. 112 (14) (2000) 6472–6486, http://dx.doi.org/10.1063/1.481208.
[32] S. Nouranian, M.A. Tschopp, S.R. Gwaltney, M.I. Baskes, M.F. Horstemeyer, An interatomic potential for saturated hydrocarbons based on the modified embedded-atom method, Phys. Chem. Chem. Phys. 16 (13) (2014) 6233–6249, http://dx.doi.org/10.1039/C4CP00027G.
[33] K. Chenoweth, A.C. Van Duin, W.A. Goddard, Reaxff reactive force field for molecular dynamics simulations of hydrocarbon oxidation, J. Phys. Chem. A 112 (5) (2008) 1040–1053, http://dx.doi.org/10.1021/jp709896w.
[34] S.J. Plimpton, A.P. Thompson, Computational aspects of many-body potentials, MRS Bull. 37 (05) (2012) 513–521, http://dx.doi.org/10.1557/mrs.2012.96.
[35] D.W. Brenner, O.A. Shenderova, J.A. Harrison, S.J. Stuart, B. Ni, S.B. Sinnott, A second-generation reactive empirical bond order (REBO) potential energy expression for hydrocarbons, J. Phys.: Condens. Matter. 14 (4) (2002) 783–802, http://dx.doi.org/10.1088/0953-8984/14/4/312.
[36] M. Daw, S. Foiles, M. Baskes, The embedded-atom method: a review of theory and applications, Mater. Sci. Rep. (September 1992) (1993) 251–310, http://dx.doi.org/10.1016/0920-2307(93)90001-U.
[37] S. Nouranian, S.R. Gwaltney, M.I. Baskes, M.A. Tschopp, M.F. Horstemeyer, Simulations of tensile bond rupture in single alkane molecules using reactive interatomic potentials, Chem. Phys. Lett. 635 (2015) 278–284, http://dx.doi.org/10.1016/j.cplett.2015.06.071.
[38] T.P. Senftle, S. Hong, M.M. Islam, S.B. Kylasa, Y. Zheng, Y.K. Shin, C. Junkermeier, R. Engel-Herbert, M.J. Janik, H.M. Aktulga, T. Verstraelen, A. Grama, A.C.T. van Duin, The reaxff reactive force-field: development, applications and future directions, Npj Comput. Mater. 2 (1) (2016) 15011, http://dx.doi.org/10.1038/npjcompumats.2015.11.
[39] A.C. Van Duin, S. Dasgupta, F. Lorant, W.A. Goddard, Reaxff: a reactive force field for hydrocarbons, J. Phys. Chem. A 105 (41) (2001) 9396–9409, http://dx.doi.org/10.1021/jp004368u.
[40] A.P. Thompson, H.M. Aktulga, R. Berger, D.S. Bolintineanu, W.M. Brown, P.S. Crozier, P.J. in 't Veld, A. Kohlmeyer, S.G. Moore, T.D. Nguyen, R. Shan, M.J. Stevens, J. Tranchida, C. Trott, S.J. Plimpton, LAMMPS - a flexible simulation tool for particle-based materials modeling at the atomic, meso, and continuum scales, "Comp. Phys. Comm." 271 (2022) 108171, http://dx.doi.org/10.1016/j.cpc.2021.108171.
[41] F. Neese, F. Wennmohs, U. Becker, C. Riplinger, The ORCA quantum chemistry program package, J. Chem. Phys. 152 (22) (2020) http://dx.doi.org/10.1063/5.0004608.
[42] F. Neese, Software update: the ORCA program system, version 5.0, WIRES Comput. Molec. Sci. 12 (1) (2022) e1606, http://dx.doi.org/10.1002/wcms.1606.
[43] A.D. Becke, Density-functional thermochemistry. III. The role of exact exchange, J. Chem. Phys. 98 (7) (1993) 5648–5652, http://dx.doi.org/10.1063/1.464913.
[44] W. Koch, M.C. Holtausen, A chemist's guide to density functional theory, second ed., Wiley-VCH, 2001.
[45] F. Weigend, R. Ahlrichs, Balanced basis sets of split valence, triple zeta valence and quadruple zeta valence quality for h to rn: Design and assessment of accuracy, Phys. Chem. Chem. Phys. 7 (18) (2005) 3297–3305, http://dx.doi.org/10.1039/B508541A.
[46] F. Weigend, Accurate Coulomb-fitting basis sets for h to rn, Phys. Chem. Chem. Phys. 8 (9) (2006) 1057–1065, http://dx.doi.org/10.1039/B515623H.
[47] F. Jensen, Introduction to computational chemistry, third ed., Wiley, 2017.
[48] S. Grimme, J. Antony, S. Ehrlich, H. Krieg, A consistent and accurate ab initio parametrization of density functional dispersion correction (DFT-d) for the 94 elements h-pu, J. Chem. Phys. 132 (15) (2010) http://dx.doi.org/10.1063/1.3382344.
[49] S. Grimme, S. Ehrlich, L. Goerigk, Effect of the damping function in dispersion corrected density functional theory, J. Comput. Chem. 32 (7) (2011) 1456–1465, http://dx.doi.org/10.1002/jcc.21759.
[50] W. Humphrey, A. Dalke, K. Schulten, VMD – visual molecular dynamics, J. Mol. Graph. 14 (1996) 33–38, http://dx.doi.org/10.1016/0263-7855(96)00018-5.
[51] J. Behler, Four generations of high-dimensional neural network potentials, Chem. Rev. 121 (16) (2021) 10037–10072, http://dx.doi.org/10.1021/acs.chemrev.0c00868.